Coupling modulation of microrings at rates beyond the linewidth limit

Article *in* Optics Express · April 2013

DOI: 10.1364/OE.21.009722 · Source: PubMed

Coupling modulation of microrings at rates beyond the linewidth limit

W. D. Sacher,[1*] **W. M. J. Green,**[2,4] **S. Assefa,**[2] **T. Barwicz,**[2] **H. Pan,**[2] **S. M. Shank,**[3] **Y. A. Vlasov,**[2] **J. K. S. Poon**[1,5]

[1]*Department of Electrical and Computer Engineering and Institute for Optical Sciences, University of Toronto, 10 King's College Road, Toronto, Ontario, M5S 3G4, Canada*
[2]*IBM Thomas J. Watson Research Center, 1101 Kitchawan Road, Yorktown Heights, New York 10598, U.S.A.*
[3]*IBM Systems and Technology Group, Microelectronics Division, 1000 River St., Essex Junction, Vermont 05452, U.S.A.*

[4]*wgreen@us.ibm.com*
[5]*joyce.poon@utoronto.ca*
**wesley.sacher@mail.utoronto.ca*

Abstract: We demonstrate optical modulation rates exceeding the conventional cavity linewidth limit using a silicon coupling modulated microring. Small-signal measurements show coupling modulation was free of the parasitic cavity linewidth limitations at rates at least $6\times$ the cavity linewidth. Eye diagram measurements show coupling modulation achieved data rates $> 2\times$ the rate attainable by conventional intracavity phase modulation. We propose to use DC-balanced encoding to mitigate the inter-symbol interference in coupling modulation. Analysis shows that coupling modulation can be more efficient than intracavity modulation for large output swings and high-Q resonators. Coupling modulation enables very high-Q resonant modulators to be simultaneously low-power and high-speed, features which are mutually incompatible in typical resonant modulators studied to date.

OCIS codes: (130.3120) Integrated optics devices; (130.4110) Modulators; (230.5750) Resonators.

References and links

1. Q. F. Xu, B. Schmidt, S. Pradhan, and M. Lipson, "Micrometre-scale silicon electro-optic modulator," Nature **435**, 325–327 (2005).
2. W. A. Zortman, A. L. Lentine, D. C. Trotter, and M. R. Watts, "Low-voltage differentially-signaled modulators," Opt. Express **19**, 26017–26026 (2011).
3. P. Dong, S. Liao, D. Feng, H. Liang, D. Zheng, R. Shafiiha, C.-C. Kung, W. Qian, G. Li, X. Zheng, A. V. Krishnamoorthy, and M. Asghari, "Low Vpp, ultralow-energy, compact, high-speed silicon electro-optic modulator," Opt. Express **17**, 22484–22490 (2009).
4. G. Li, X. Zheng, J. Yao, H. Thacker, I. Shubin, Y. Luo, K. Raj, J. E. Cunningham, and A. V. Krishnamoorthy, "25 Gb/s 1 V-driving cmos ring modulator with integrated thermal tuning," Opt. Express **19**, 20435–20443 (2011).
5. X. Xiao, X. Li, H. Xu, Y. Hu, K. Xiong, Z. Li, T. Chu, J. Yu, and Y. Yu, "44-Gb/s silicon microring modulators based on zigzag PN junctions," IEEE Photon. Technol. Lett. **24**, 1712–1714 (2012).
6. W. Zortman, D. Trotter, A. Lentine, G. Robertson, A. Hsia, and M. Watts, "Monolithic and two-dimensional integration of silicon photonic microdisks with microelectronics," IEEE Photonics Journal **4**, 242 –249 (2012).
7. J. C. Rosenberg, W. M. J. Green, S. Assefa, D. M. Gill, T. Barwicz, M. Yang, S. M. Shank, and Y. A. Vlasov, "A 25 Gbps silicon microring modulator based on an interleaved junction," Opt. Express **20**, 26411–26423 (2012).

#184796 - $15.00 USD Received 5 Feb 2013; revised 5 Apr 2013; accepted 5 Apr 2013; published 12 Apr 2013

8. P. Rabiei, W. H. Steier, C. Zhang, and L. R. Dalton, "Polymer micro-ring filters and modulators," J. Lightwave Technol. **20**, 1968–1975 (2002).
9. W. D. Sacher and J. K. S. Poon, "Dynamics of microring resonator modulators," Opt. Express **16**, 15741–15753 (2008).
10. W. D. Sacher and J. K. S. Poon, "Characteristics of microring resonators with waveguide-resonator coupling modulation," J. Lightwave Technol. **27**, 3800–3811 (2009).
11. A. Yariv, "Critical coupling and its control in optical waveguide-ring resonator systems," IEEE Photon. Technol. Lett. **14**, 483–485 (2002).
12. W. M. J. Green, R. K. Lee, G. A. DeRose, A. Scherer, and A.Yariv, "Hybrid InGaAsP-InP Mach-Zehnder racetrack resonator for thermooptic switching and coupling control," Opt. Express **13**, 1651–1659 (2005).
13. L. Zhou and A. W. Poon, "Electrically reconfigurable silicon microring resonator-based filter with waveguide-coupled feedback," Opt. Express **15**, 9194–9204 (2007).
14. D. Gill, S. Patel, M. Rasras, K.-Y. Tu, A. White, Y.-K. Chen, A. Pomerene, D. Carothers, R. Kamocsai, C. Hill, and J. Beattie, "CMOS-compatible Si-ring-assisted Mach-Zehnder interferometer with internal bandwidth equalization," IEEE J. Sel. Top. Quant. Elect. **16**, 45 –52 (2010).
15. P. Dong, L. Chen, Q. F. Xu, and M. Lipson, "On-chip generation of high-intensity short optical pulses using dynamic microcavities," Opt. Lett. **34**, 2315–2317 (2009).
16. D. Gill, M. Rasras, K.-Y. Tu, Y.-K. Chen, A. White, S. Patel, D. Carothers, A. Pomerene, R. Kamocsai, C. Hill, and J. Beattie, "Internal bandwidth equalization in a CMOS-compatible Si-ring modulator," IEEE Photon. Technol. Lett. **21**, 200 –202 (2009).
17. W. Sacher, W. Green, S. Assefa, T. Barwicz, S. Shank, Y. Vlasov, and J. Poon, "Controlled coupling in silicon microrings for high-speed, high extinction ratio, and low-chirp modulation," in "Conference on Lasers and Electro-Optics (CLEO)," (2011), PDPA8.
18. R. Soref and B. Bennett, "Electrooptical effects in silicon," IEEE J. Quant. Elect. **23**, 123–129 (1987).
19. A. A. Savchenkov, A. B. Matsko, V. S. Ilchenko, D. Seidel, and L. Maleki, "Surface acoustic wave opto-mechanical oscillator and frequency comb generator," Opt. Lett. **36**, 3338–3340 (2011).
20. S. Assefa, W. Green, A. Rylyakov, C. Schow, F. Horst, and Y. Vlasov, "CMOS integrated nanophotonics-enabling technology for exascale computing systems," in "Optical Fiber Communication Conference (OFC/NFOEC)," (2011), OMM6.
21. S. Assefa, S. M. Shank, W. M. J. Green, M. Khater, E. Kiewra, C. Reinholm, S. Kamlapurkar, A. Rylyakov, C. Schow, F. Horst, H. Pan, T. Topuria, P. Rice, D. M. Gill, J. Rosenberg, T. Barwicz, M. Yang, P. Proesel, J. Hofrichter, B. Offrein, . Gu, W. Haensch, J. Ellis-Monaghan, and Y. Vlasov, "A 90 nm CMOS integrated nano-photonics technology for 25 Gbps WDM optical communications applications," in "IEEE International Electron Devices Meeting (IEDM)," (2012), 33.8.1–33.8.3.
22. Q. F. Xu, S. Manipatruni, B. Schmidt, J. Shakya, and M. Lipson, "12.5 Gbit/s carrier-injection-based silicon micro-ring silicon modulators," Opt. Express **15**, 430–436 (2007).
23. W. M. J. Green, M. J. Rooks, L. Sekaric, and Y. A. Vlasov, "Ultra-compact, low RF power, 10 Gb/s silicon Mach-Zehnder modulator," Opt. Express **15**, 17106–17113 (2007).
24. S. Manipatruni, Q. F. Xu, B. Schmidt, J. Shakya, and M. Lipson, "High speed carrier injection 18 Gb/s silicon micro-ring electro-optic modulator," in "The Annual Meeting of the IEEE Lasers and Electro-Optics Society," (2007), 537 –538.
25. M. A. Popovic, "Resonant optical modulators beyond conventional energy-efficiency and modulation frequency limitations," in "Integrated Photonics Research, Silicon and Nanophotonics," (2010), IMC2.
26. H. Lee, T. Chen, J. Li, K. Y. Yang, S. Jeon, O. Painter, and K. J. Vahala, "Chemically etched ultrahigh-Q wedge-resonator on a silicon chip," Nature Photonics **6**, 369–373 (2012).
27. W. D. Sacher and J. K. S. Poon, "Microring quadrature modulators," Opt. Lett. **34**, 3878–3880 (2009).
28. W. D. Sacher, E. J. Zhang, B. A. Kruger, and J. K. S. Poon, "High-speed laser modulation beyond the relaxation resonance frequency limit," Opt. Express **18**, 7047–7054 (2010).

1. Introduction

Microring optical modulators have been studied extensively in recent years because they can significantly reduce the power consumption and device footprint of optical transmitters via the resonant circulation of light [1–7]. A microring modulator, in its simplest form, consists of a closed waveguide loop coupled to an input/output waveguide. A constant light beam is the input, and a parameter of the microring is modulated to produce a time-varying optical output.

Two distinct operation modes are intracavity and coupling modulation. The vast majority of microring modulators to date use intracavity modulation (Fig. 1(a)), where the circulating optical field is modulated by the intracavity round-trip phase, $\phi(t)$, and/or loss, $a(t)$, while

#184796 - $15.00 USD Received 5 Feb 2013; revised 5 Apr 2013; accepted 5 Apr 2013; published 12 Apr 2013

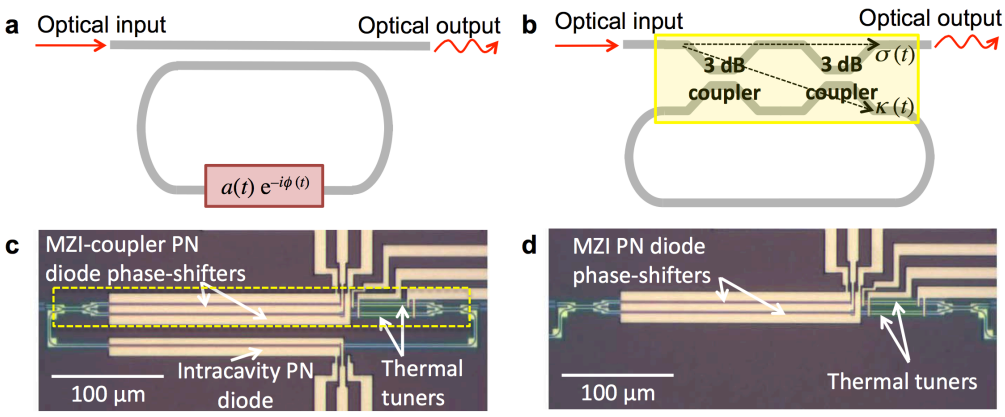

Fig. 1. Schematics of (a) an intracavity modulated microring and (b) a coupling modulated microring that uses a 2×2 MZI-coupler as marked by the box. Optical microscope images of the fabricated SOI (c) microring with the 2×2 MZI-coupler marked by the box and (d) the reference MZI. The reference MZI was nominally identical to the MZI-coupler in the microring. The microring and MZI were separated by 620 μm on the die.

the coupler is fixed [1–8]. Because the intracavity optical field amplitude rises and falls at a time-scale set by the photon cavity lifetime, the maximum intracavity modulation bandwidth diminishes with increasing Q [9]. Additionally, complete on/off modulation (0-100% transmission) requires the stored intracavity optical energy be completely charged and depleted in each switching cycle. Thus, whether in the small- or large- output signal regime, the intracavity modulation bandwidth is inherently limited by the cavity linewidth.

Coupling modulation circumvents this linewidth limitation. In coupling modulation, the intracavity parameters, ϕ and a, remain constant, while the through- and cross-coupling coefficients, $\sigma(t)$ and $\kappa(t)$ respectively, are modulated (Fig. 1(b)) [9, 10]. We term the regime where the modulation rate is greater than the cavity linewidth "non-quasi-static (NQS) coupling modulation" [10]. "Quasi-static (QS) coupling modulation" refers to modulation rates less than the linewidth, when the output can be described by simply changing the expression for the static transmission to be time-dependent [11–14].

Distinct from the QS regime, intracavity modulation, and Q-switching (cavity dumping) [15], NQS coupling modulation does not completely deplete the intracavity optical energy to generate near 0-100% transmission swings. Instead, it extracts, in the transient, minor fractions of the intracavity optical field in a high finesse cavity to produce output optical pulses with peak powers that can equal the input optical power. The coupler gates the intracavity optical field as it exits the microring to enable NQS coupling modulation bandwidth to exceed the cavity linewidth [10]. The effect is akin to "homodyne modulation," where the circulating resonant light is the "local oscillator." NQS coupling modulation is resonantly enhanced, since the required changes to the coupling coefficients, and hence the device power consumption, reduce as the stored intracavity optical energy increases [10].

In this article, we demonstrate NQS coupling modulation using a silicon microring incorporating a 2×2 Mach-Zehnder interferometer (MZI) as a coupler, as illustrated in Fig. 1(b) [11–14, 16]. The MZI-coupler provides independent control of the coupling coefficient and resonance wavelength. The differential phase-shift between the MZI-coupler arms changes $\kappa(t)$ and $\sigma(t)$ [11,12], while the common-mode phase-shift changes the round-trip optical path length. When the MZI is driven in push-pull mode, the microring has no chirp beyond that of the material (i.e., free carrier dispersion in silicon) [10, 17, 18]. Although periodic modulation

#184796 - $15.00 USD Received 5 Feb 2013; revised 5 Apr 2013; accepted 5 Apr 2013; published 12 Apr 2013

at rates greater than linewdith due to a slight variation of the coupling coefficient has been recently observed [19], data modulation has not been studied.

The paper is organized as follows. In Section 2, we describe the fabricated devices. In Sections 3 and 4, we present small-signal and eye diagram measurements comparing intracavity and coupling modulation to clearly show that coupling modulation enables modulation rates exceeding the cavity linewidth limit, while intracavity modulation does not. In Section 5, we discuss how inter-symbol interference in coupling modulation due to the low frequency content in the modulation signal can be overcome with coding. Finally, in Section 6, we compare the theoretical efficiency of coupling and intracavity modulation to show the regimes where coupling modulation has a lower energy consumption.

2. Fabricated devices

Microring and reference MZI modulators were fabricated using the IBM Silicon CMOS Integrated Nanophotonics process on a 200 mm-diameter silicon-on-insulator (SOI) wafer with a 2 μm-thick buried-oxide layer and a 220 nm-thick top silicon layer [20,21] . Fully-etched silicon access waveguides and partially-etched PN diode waveguides were defined and planarized with silicon dioxide through a shallow trench isolation module. Typical CMOS ion implantation conditions formed a lateral PN diode junction at the center of each phase-shifter. The junction was designed with a nominal carrier concentration of 5×10^{17} cm^{-3} in the P- and N-type regions. After a rapid thermal activation anneal, silicide ohmic contacts to the phase-shifters and silicide resistive thermal tuners were formed. Finally, tungsten vias and copper metal interconnects electrically contacted the phase-shifters and thermal tuners. Dies were prepared with cleaved facets for on/off-chip optical coupling using tapered optical fibers.

Figure 1(c) shows the specific microring investigated. The microring was designed for exploring the optical dynamics and was not optimized for power consumption. The 2×2 MZI-coupler had 3 dB directional couplers, 50 μm long thermal tuners, and matched 200 μm long PN diode phase-shifters for push-pull modulation. An identical PN diode phase-shifter was included inside the microring to facilitate direct comparisons between intracavity and coupling modulation with the same device.

The PN diode phase-shifter length was chosen such that a reference MZI, which is nominally identical to the output coupler of the microring (i.e., designed to have identical waveguides, PN diode phase-shifters, thermal tuners, and wiring), could be measured (see Sections 3 and 4). Figure 1(d) shows the reference MZI for the microring in Fig. 1(c). The reference MZI and microring modulator were on the same die and separated by about 620 μm.

Figures 2(a)-2(b) shows the static transmission spectra of the microring. The results demonstrate the precise and independent tuning of the coupling coefficient and resonance wavelength, achieved by adjusting the thermal tuners to create a common or differential phase-shift in the MZI-coupler arms. An extinction ratio near 30 dB was reached at critical coupling. With no voltage applied to the PN diode phase-shifters, the cavity linewidth at critical coupling was $\Delta\nu \approx 7$ GHz, corresponding to a loaded Q of about 28000 and a finesse of 14.

3. Small-signal modulation measurements

To extract the small-signal optical modulation characteristics of coupling and intracavity modulation, we measured electro-optic S_{21} parameters by collecting the voltage of a 40 GHz InGaAs photoreceiver referenced to a vector network analyzer (VNA) output. For coupling modulation, the MZI phase-shifters in the microring were driven in push-pull. To generate a differential drive signal, the VNA output was fed into a fanout circuit (Hittite HMC842LC4B), which had a bandwidth of about 32 GHz. For intracavity modulation, a single-ended signal generated from the VNA was applied to the intracavity phase-shifter without the fanout. Custom 40 GHz RF

#184796 - $15.00 USD Received 5 Feb 2013; revised 5 Apr 2013; accepted 5 Apr 2013; published 12 Apr 2013

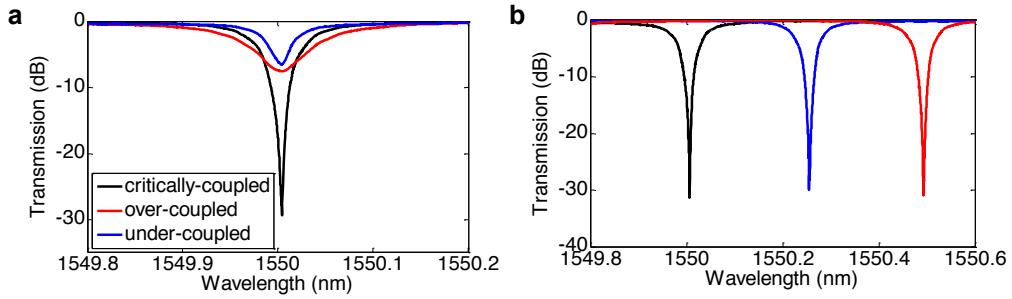

Fig. 2. Measured transmission spectra for (a) tuning the coupling coefficient at a fixed resonance and (b) tuning the resonance wavelength with a fixed coupling coefficient. Independent tuning of the coupling and resonance wavelength using the thermal tuners was achieved.

probes contacted the devices.

Figure 3(a) shows the measured S_{21} of the reference MZI as well as the microring operated under coupling and intracavity modulation modes. Each curve is referenced to its value at 100 MHz. The responses of the RF cables, RF adapters, and bias tees were de-embedded from the S_{21} data; however, the responses of the fanout, RF probes, and on-chip wiring remained embedded. The S_{21} of the reference MZI when driven in push-pull used the fanout, while the fanout was not used for for the single-arm drive measurement. This led to slight differences in the S_{21} between the two cases. The reference MZI was baised at quadrature using the thermal tuners to maximize the modulation efficiency of the MZI and reduce the relative noise in the measurements. Experimentally, we found that the shape of the reference MZI S_{21} curves was insensitive to changes in the MZI bias. The coupling modulation S_{21} measurements were taken with the input wavelength on resonance and a slightly under-coupled bias. The intracavity modulation S_{21} measurements were taken at critical coupling with the input wavelength roughly 1.3 GHz and 5 GHz detuned from resonance to obtain an appreciable modulation depth. In all cases, the PN diode phase-shifters were biased at -1 V.

To extract the small-signal modulation response due to the optical cavity dynamics, we normalize the electro-optic S_{21} parameter of the microring modulator to the electro-optic S_{21} of the reference MZI to remove the electrical characteristics of the measurement setup, on-chip wiring, and PN diode phase-shifters. The normalized coupling modulation response, S_{cm}, and normalized intracavity modulation response, S_{im}, are given by

$$\mathsf{S}_{\mathsf{cm}} = \frac{S_{21,cm}}{S_{21,MZI,push-pull}}, \tag{1a}$$

$$\mathsf{S}_{\mathsf{im}} = \frac{S_{21,im}}{S_{21,MZI,single}}, \tag{1b}$$

where $S_{21,MZI,push-pull}$ and $S_{21,MZI,single}$ are the electro-optic S_{21} of the reference MZI under push-pull and single-arm drive, respectively; and $S_{21,cm}$ and $S_{21,im}$ are the electro-optic S_{21} of the coupling and intracavity modulation, respectively. $S_{21,MZI,push-pull}$, $S_{21,MZI,single}$, $S_{21,cm}$, and $S_{21,im}$ are as shown in Fig. 3(a).

Figure 3(b) shows the small-signal optical modulation characteristics, S_{cm} and S_{im}. The coupling modulation bandwidth significantly exceeds the traditional cavity linewidth limit, while intracavity modulation does not. Under bias, the microring had a cavity linewidth of $\Delta\nu \approx 6$ GHz. The black curve in Fig. 3 shows the coupling modulation response did not roll off to 40 GHz, more than $6\times$ the cavity linewidth. The maximum frequency measured was limited by

#184796 - $15.00 USD Received 5 Feb 2013; revised 5 Apr 2013; accepted 5 Apr 2013; published 12 Apr 2013

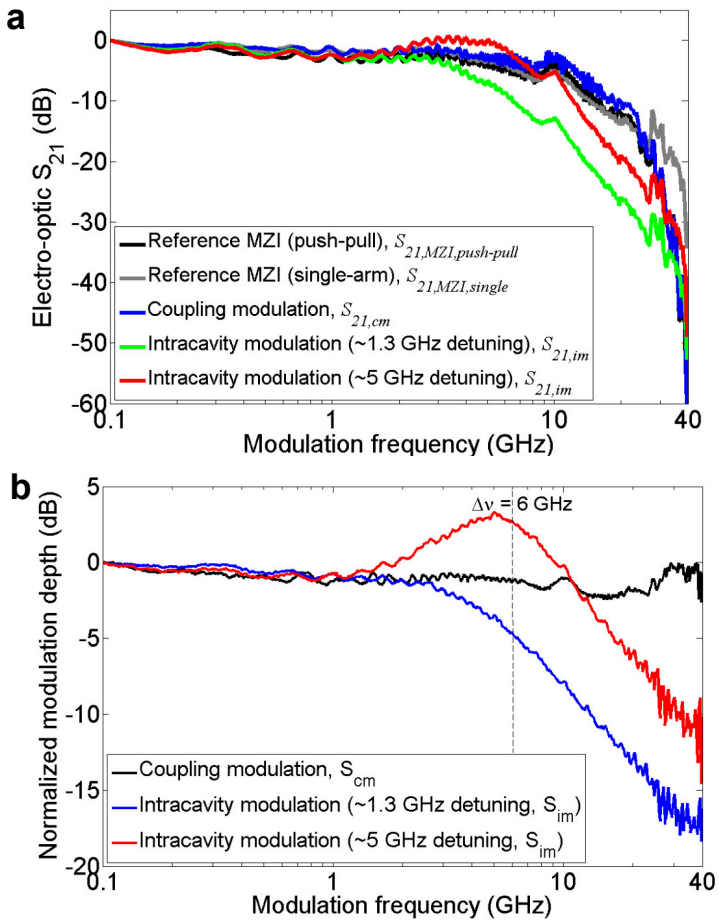

Fig. 3. (a) Electro-optic S_{21} measurements of the reference MZI, coupling modulation, and intracavity modulation. The RF cables, RF adapters, and bias tees have been de-embedded. (b) Optical small-signal modulation responses of coupling and intracavity modulation. Each curve is obtained by normalizing the electro-optic S_{21} of the microring to the S_{21} of the reference MZI and referencing to the value at 100 MHz. The microring was biased near critical coupling, with a cavity linewidth $\Delta\nu \approx 6$ GHz. The intracavity modulation response for a ~ 1.3 GHz detuning from resonance (blue) has a 3 dB bandwidth of 4.4 GHz, similar to the linewidth. A ~ 5 GHz detuning produces a resonant sideband peak near the value of the detuning (red), and the 3 dB bandwidth is extended to ~ 13 GHz. The coupling modulation response (black) does not roll-off to 40 GHz (more than $6\times$ the linewidth).

#184796 - $15.00 USD Received 5 Feb 2013; revised 5 Apr 2013; accepted 5 Apr 2013; published 12 Apr 2013

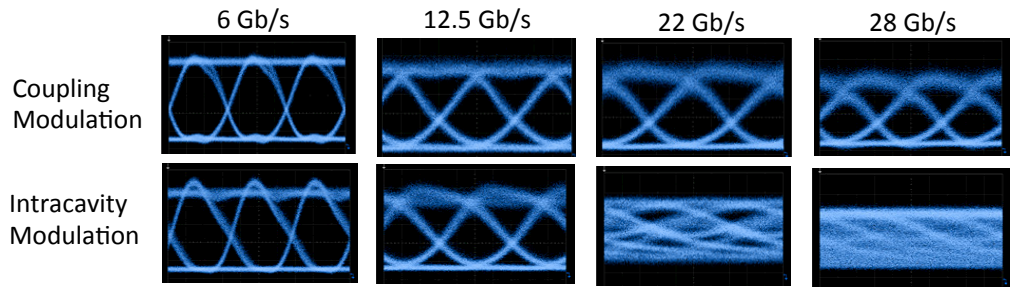

Fig. 4. Eye diagrams of coupling (top) and intracavity (bottom) modulation at 6-28 Gb/s for bias points near critical coupling ($\Delta\nu \approx 6-7$ GHz). The coupling modulation eye is open at 28 Gb/s, but the intracavity modulation eye closes at bit rates greater than roughly $2\times$ the linewidth.

the instrumentation. The flat response indicates that the frequency characteristics of the NQS coupling modulation resembled those of the non-resonant reference MZI. The slight decrease in the modulation depth near the frequency corresponding to the cavity linewidth was due to a slight under-coupling of the microring [9].

In contrast, the intracavity modulation response with input light that was 1.3 GHz detuned from resonance (blue curve) had a 3 dB bandwidth of about 4.4 GHz, confirming that the intrinsic modulation bandwidth was limited by the cavity linewidth. For larger detunings, a peak occurs when a modulation sideband is on resonance and becomes comparable to or greater than the carrier in amplitude within the microring [9, 14, 16]. The peak is exaggerated for large detunings, because the circulating amplitude of an off-resonant carrier is small. This effect is shown by the ~ 5 GHz detuning measurement (red curve). Although the modulation sideband peak extended the 3 dB bandwidth to about 13 GHz, intracavity modulation of a highly detuned carrier is not practical, because the absolute modulation depth and the linearity of the modulator are compromised.

4. PRBS modulation and eye diagram measurements

Large-signal data modulation and optical eye diagram measurements provide further evidence that the coupling modulation bandwidth is not similarly limited by the cavity linewidth as intracavity modulation. To reduce the required drive voltage, the PN diode phase-shifters were in forward bias, with a DC offset of 0.28 V, and driven by single-tap pre-emphasized non-return-to-zero (NRZ) $2^{31}-1$ pseudo-random bit sequence (PRBS) signals. The electrical pre-emphasis extended the modulation bandwidth of the PN diode phase-shifters beyond their minority carrier lifetime limit of ~ 1 GHz [22–24]. The drive signals were generated by feeding the output of a PRBS generator to a pre-emphasis converter which operated up to 28 Gb/s (Anritsu MP1825B-002), and then to the RF probes. The applied single-ended voltage swing of the pre-emphasized bits was 1.5 V_{pp}, and the non-emphasized bits were between 0.24-0.3 V_{pp}.

To measure the eye diagrams, the optical output of the modulator was amplified using an erbium doped fiber amplifier, bandpass filtered (full-width at half-maximum bandwidth of 0.8 nm), and captured on a digital communications analyzer with a 28 Gb/s optical module. All eye diagrams were obtained using $2^{31}-1$ PRBS.

Figure 4 summarizes the coupling and intracavity modulation eye diagrams at bit rates between 6 and 28 Gb/s. The cavity linewidths at the operating biases were $\Delta\nu \approx 6-7$ GHz. At each bit rate, identical drive signals were applied to the coupler or intracavity phase-shifters, except the MZI-coupler was driven in push-pull while the intracavity phase-shifter was driven

#184796 - $15.00 USD Received 5 Feb 2013; revised 5 Apr 2013; accepted 5 Apr 2013; published 12 Apr 2013

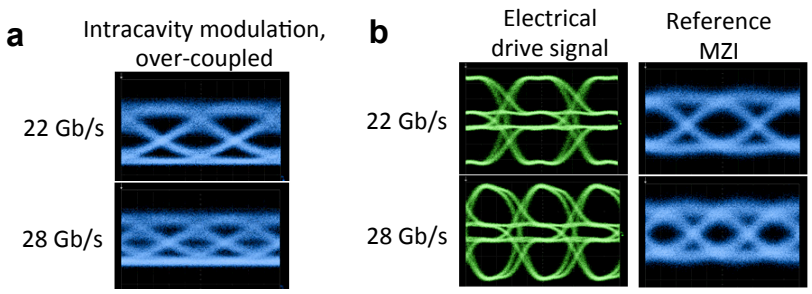

Fig. 5. (a) Intracavity modulation eye diagrams of an over-coupled microring ($\Delta\nu \approx 9$ GHz). The eye opening is larger than in Fig. 4, confirming that the intracavity modulation bandwidth depends on the cavity linewidth. (b) Eye diagrams of the pre-emphasized electrical drive signals at 28 Gb/s (left) and the resultant optical output of the reference MZI (right). No remnants of the pre-emphasis are present in the optical output.

single-ended. For coupling modulation, the microring was modulated between critical and under- coupling with the input light on resonance. For intracavity modulation, the microring was biased at critical coupling and the input wavelength was slightly detuned from resonance. Thus, the quasi-static cavity linewidth for coupling modulation was less than or equal to that for the corresponding intracavity modulation case. The pre-emphasis ratio and detuning were optimized to maximize the eye opening for each case.

At 6 Gb/s and 12.5 Gb/s, both the coupling and intracavity modulation eye diagrams had extinction ratios of 10-13 dB and a maximum optical transmission $> 40\%$. As the bit rate increased, the coupling modulation eye remained wide open up to 28 Gb/s, whereas the intracavity modulation eye was closed at 22 Gb/s. However, because of the modest finesse and the roll-off of the PN diode phase-shifter efficiency at high modulation frequencies, the extinction ratio of coupling modulation at 22 Gb/s and 28 Gb/s decreased to 10 dB, and the maximum optical transmission was only about 10 to 20% of the off-resonance transmission. At 28 Gb/s, the peak-to-peak phase-shift in each PN diode phase-shifter was about 0.18 rad., and the coupler swung between $|\kappa|^2 \approx 0.2$ and $|\kappa|^2 \approx 0.08$.

The reduction in maximum optical transmission at high data rates is not necessarily a characteristic of coupling modulation. As discussed in Section 5 and [10], near unity transmission is achievable, particularly when the bit rate is much higher than the linewidth and when the stored optical energy in the cavity is not significantly depleted during modulation. The Q factor of the modulator here was compromised by the intracavity PN diode phase-shifter, which was necessary to compare the dynamics of intracavity and coupling modulation. Nonetheless, coupling modulation of the demonstrated microring should function beyond 28 Gb/s. The measurements were limited by the instrumentation.

To check that the intracavity modulation eye closure was due to the cavity linewidth and not to an electrical artifact, we over-coupled the microring by adjusting the thermal tuners to increase the linewidth to 9 GHz at the expense of modulator efficiency and extinction ratio. Figure 5(a) shows that the eye opening increased at 22 Gb/s, but remained closed at 28 Gb/s. The eye diagrams show that intracavity modulation suffered from severe inter-symbol interference at bit rates greater than roughly $2\times$ the cavity linewidth (i.e. > 12.5 Gb/s), while coupling modulation at up to $4\times$ the linewidth was not similarly affected.

To determine that the pre-emphasized drive signals only compensated for the modulation bandwidth of the PN diodes, we measured the optical output of the reference MZI. Figure 5(b) (left) shows the eye diagram of the pre-emphasized 28 Gb/s drive signal. The optical output of the reference MZI driven with this signal in push-pull mode (Fig. 5(b), right) shows that the

#184796 - $15.00 USD Received 5 Feb 2013; revised 5 Apr 2013; accepted 5 Apr 2013; published 12 Apr 2013

MZI-coupler optical output did not contain any remnants of the pre-emphasis in the drive signal which could potentially extend the microring modulation bandwidth beyond the limits of the resonant optical dynamics.

Because the PN diodes were swinging between forward and reverse biased states, the dynamic power consumption of the device was difficult to estimate. To obtain an upper-bound to the power consumption, we directly measured the average dynamic power incident on the probes using a RF power detector. For the measurements at 28 Gb/s (Fig. 4), this power was about 750 fJ/bit. The device dynamic power consumption was likely less due to the impedance mismatch and RF reflection between the modulator and the test equipment. This measured power consumption is not a fundamental limitation of the MZI-microring geometry. The power consumption can be reduced by replacing the thermal tuners with a length mismatch in the MZI as in [13], shortening the MZI PN diode phase-shifters, removing the intracavity PN diode, increasing the Q factor and improving the diode efficiency.

5. Overcoming low frequency distortions in coupling modulation

The results in Sections 3 and 4 clearly demonstrate that the long-held cavity linewidth limit to the intracavity modulation bandwidth can be broken with coupling modulation. However, a potential drawback to coupling modulation is the inter-symbol interference (ISI) from the *low* frequency content of the drive signal, which depletes the stored optical energy in the cavity. To mitigate the ISI, one suggestion is to modulate two couplers to maintain a constant intracavity optical power at the expense of device complexity, cavity finesse, and power efficiency for large-signal modulation [25].

As a more straight-forward alternative, we propose to encode the electrical data to produce a DC-balanced drive signal. An example is the 8b/10b code, a typical line code for Ethernet and InfiniBand standards. The computed eye diagrams in Fig. 7(a) illustrate the effect of the encoding at bit rates from 2 Gb/s to 100 Gb/s. The simulations use a NRZ PRBS $2^{17}-1$ pattern, a 5 GHz cavity linewidth, and a 250 μm round-trip length.

The top row shows that uncoded intracavity modulation requires a linewidth that is at least half the bit rate, in agreement with our measurements. The middle row shows that for uncoded non-quasi-static (NQS) coupling modulation at 40 Gb/s and 100 Gb/s, the transmission swing in the eye opening is about 25%, and increasing the amplitude of the drive signals would increase the ISI since more energy would be discharged from the cavity. As in our experiment, the resonator in the calculation is driven between under- and critical coupling. NQS coupling modulation in the over-coupled regime incurs more ISI due to the increased discharge of the stored optical energy [9, 10], but it can generate pulses with peak powers greater than the input power [15] similar to intracavity modulation in the top row. At a fixed modulation rate, microrings with narrower linewidths would improve the eye opening for uncoded NQS coupling modulation, since the circulating energy would be higher, and a smaller fraction of the circulating energy would be discharged to form the output. The bottom row shows that an 8b/10b encoded drive signal enables NQS coupling modulation at 40 Gb/s and 100 Gb/s to have an eye opening of about 90% and low ISI at 100 Gb/s, characteristics not possible with intracavity modulation. Importantly, the coupling modulation ISI diminishes as the bit rate increases, since the low frequency content of the modulation signal is reduced.

6. Analysis of the modulation efficiency

Although our results show that the coupling modulation bandwidth can be substantially larger than the intracavity modulation bandwidth, an essential question is whether coupling modulation of a narrow linewidth resonator can be more power efficient than intracavity modulation of a small resonator with a broad linewidth. In practice, both types of modulation may require

#184796 - $15.00 USD Received 5 Feb 2013; revised 5 Apr 2013; accepted 5 Apr 2013; published 12 Apr 2013

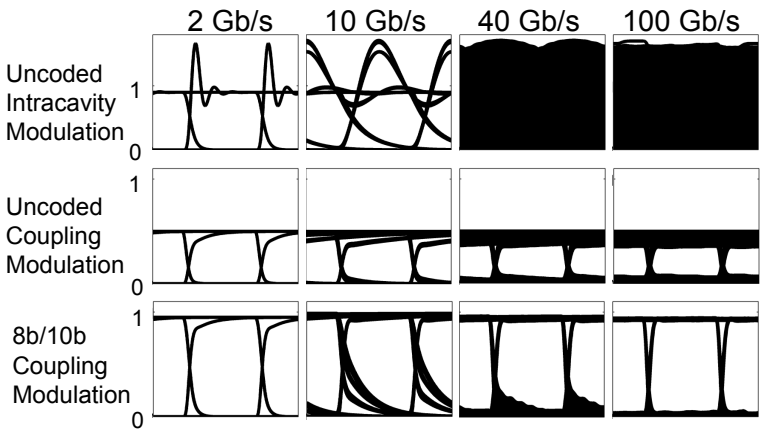

Fig. 6. Computed eye diagrams at several bit rates for (top) intracavity modulation and (center) coupling modulation driven by an uncoded NRZ signal, and (bottom) coupling modulation driven by a NRZ 8b/10b encoded signal. The calculations assume a group index of 4.3, a NRZ PRBS $2^{17}-1$ data signal, $\Delta\nu = 5$ GHz, a round-trip length of 250 μm, a resonant input for coupling modulation, and critical coupling for intracavity modulation. With DC-balanced encoding, coupling modulation can achieve a 0-90% swing at 100 Gb/s. In contrast to intracavity modulation, the DC-balanced encoded coupling modulation eye diagram becomes more open at high bit rates.

some encoding, pre-distortion, or equalization energy overhead; therefore, here, we seek to determine and compare the fundamental, optical efficiency scaling of coupling and intracavity modulation. The analysis shows that coupling modulation can indeed be more efficient for high bit rate and large-signal modulation using high-Q resonators.

We define an efficiency metric,

$$\eta = \frac{\Delta\phi_{MZI}}{\Delta\phi_{ring}}, \tag{2}$$

where $\Delta\phi_{ring}$ and $\Delta\phi_{MZI}$ are respectively the phase-shifts of a microring and a MZI biased at quadrature required to produce the same output transmission swing, assuming identical phase-shifters. $\Delta\phi$ is single-ended for intracavity modulation and is applied push-pull as $\pm\Delta\phi/2$ for coupling modulation. Referencing to $\Delta\phi_{MZI}$ allows for a comparison between coupling and intracavity modulation independent of material platforms. The phase-shifts are related to the power consumption by the electro-optic mechanism and associated drive circuitry.

For intracavity modulation, from the microring transmission function [11], the efficiency, η_i, is roughly proportional to the *intracavity power* or finesse, F:

$$\eta_i \approx k_i F, \tag{3}$$

where $k_i \lesssim 0.42$ depends on the high and low transmission levels, and the ratio of the round-trip loss to the coupling. k_i can be computed from the static transmission of a microring [11]. For example, at critical coupling and $F \gtrsim 5$, $k_i = 0.24$ for a 0-90% output swing and $k_i = 0.41$ for a 20-30% swing. k_i is lower for in the large-signal modulation regime because the microring transmission spectrum flattens at wavelengths detuned from the resonance.

In contrast, the efficiency of coupling modulation, η_c, scales with the *intracavity field*. For a MZI-coupler and a resonant input,

$$\eta_c \approx k_c \sqrt{F}, \tag{4}$$

#184796 - $15.00 USD Received 5 Feb 2013; revised 5 Apr 2013; accepted 5 Apr 2013; published 12 Apr 2013

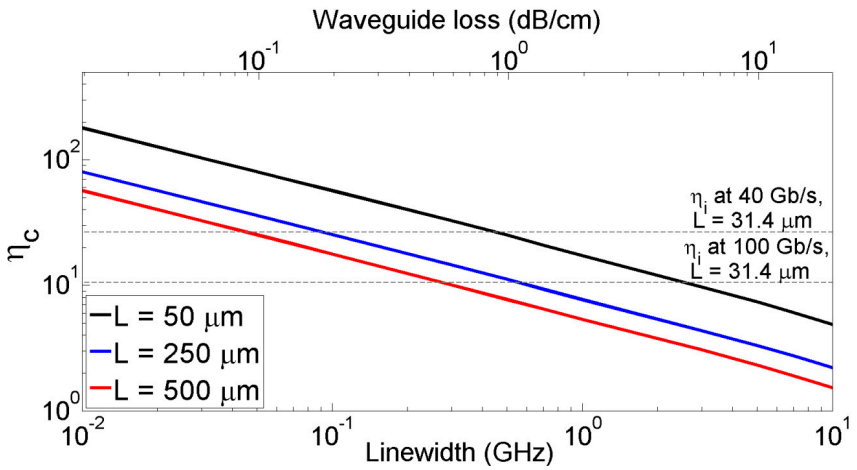

Fig. 7. The coupling modulation efficiency, η_c, versus microring waveguide loss and cavity linewidth computed for several round-trip lengths, L. The calculations assume a 8b/10b encoded drive signal, a 0-90% output swing, a group index of 4.3, a NRZ PRBS $2^{17}-1$ data signal, a resonant input, and critical coupling. The intracavity efficiency, η_i, of a 5 μm radius microring with the same output swing at 40 Gb/s and 100 Gb/s, using linewidths of 20 GHz and 50 GHz respectively, are marked for comparison. Critical coupling is assumed. Coupling modulation becomes increasingly efficient over intracavity modulation as the Q factor and bit rate increase.

where $k_c \lesssim 1$ depends on the transmission levels and F is the finesse at critical coupling. For the same transmission levels, k_c is smaller in the NQS than quasi-static (QS) regime due to a lower intracavity field. In the QS case, k_c can again be computed from the static microring transmission. For example, for $F \gtrsim 5$, $k_c = 0.85$ for a 0-90% output swing and $k_c = 0.73$ for a 20-30% swing. In the NQS regime, we derived an analytic form for k_c by assuming a periodic square-wave drive signal and solved for the average intracavity field with a rate equation. The approximation neglects the shape and low-frequency content of the drive signal. We found that in the NQS regime, $F \gtrsim 20$, $k_c = 0.41$ for a 0-90% output swing.

From Eq. 3 and 4, QS coupling modulation is more efficient than intracavity modulation in cavities with the same F and phase-shifters when $F \lesssim (k_c/k_i)^2$. Intracavity modulation is more efficient in the small-signal regime if the resonator has a moderate finesse (e.g. 20-30% swing, $F \gtrsim 5$), but QS coupling modulation is more efficient for large-signal modulation; e.g. $\eta_c > \eta_i$ for a 0-90% output swing when $F \lesssim 10$ and for a 0-99% swing when $F \lesssim 87$.

The efficiency scaling becomes especially favourable to NQS coupling modulation over intracavity modulation at high Q factors and high bit rates. Because the minimum cavity linewidth is set by the desired modulation rate, improvements in η_i of intracavity modulation via F must come from the cavity size reduction. However, tuning structures needed for large extinction ratios and large-signal swings are difficult to incorporate into ultra-small cavities. Thus, the advantage of coupling modulated microrings is that they can be kept larger (to accommodate tunable couplers), while η_c can, in principle, be arbitrarily boosted by increasing Q to raise the finesse.

Figure 7 shows the scaling of η_c for several round-trip lengths assuming a 0-90% output swing calculated using the microring modulator model in [9, 10]. The values of η_i for SOI microrings with a 5 μm radius and the same output swings at 40 Gb/s and 100 Gb/s are marked. As the round-trip length of a coupling-modulated microring increases, a narrower linewidth is

#184796 - $15.00 USD Received 5 Feb 2013; revised 5 Apr 2013; accepted 5 Apr 2013; published 12 Apr 2013

required for $\eta_c > \eta_i$.

In principle, both the modulation quality (e.g., eye opening) and energy efficiency of coupling modulation improve as the resonator linewidth decreases relative to the modulation rate if the modulation is DC balanced. However, modulation rates approaching the free spectral range (FSR) can cause distortion in the output optical signal, since the modulation time-scale would be similar to or shorter than the resonator round-trip time. In microrings, the FSRs are usually $\gtrsim$ 100 GHz, so typical modulation rates are much lower than the FSR. A second limitation is the onset of optical nonlinearities, e.g., frequency generation or absorption, in the resonator, which may occur at sub-mW input powers if the finesse is high. The input laser power should be kept to less than the nonlinearity threshold, which reduces the maximum output power.

7. Conclusion

We have demonstrated experimentally that coupling modulation circumvents the conventional limit on the maximum modulation rate of microcavities due to the photon cavity lifetime. The result is substantiated by small-signal sinusoidal and large-signal bit stream modulation measurements. We have proposed DC-balanced coding as a way to mitigate low frequency inter-symbol interference in coupling modulation. In the quasi-static regime, coupling modulation is more energy efficient than intracavity modulation when large output swings are required. In the non-quasi-static regime, coupling modulation has higher energy efficiencies compared to intracavity modulation when the cavity Q factor is high.

By combining the benefits of resonant enhancement with the large bandwidths of non-resonant modulators, coupling modulation, for the first time, opens the avenue toward ultra-low power yet high-speed modulation of ultra-high-Q resonators. Such resonators on silicon chips can possess finesse values exceeding 10000 [26]. Although a silicon microring was used in this demonstration, we emphasize that the results presented here apply generally to other types of monolithically or hybrid integrated photonic platforms. Coupling modulation of resonators can also be used to generate modulation formats besides NRZ/RZ on-off keying, such as phase-shift keying and quadrature amplitude modulation [27], as well as to achieve high-speed modulation of lasers [28] and other types of oscillators.

Acknowledgments

W.D.S. and J.K.S.P. thank the University of Toronto Emerging Communications Technology Institute for access to the VNA and RF signal generators. W.M.J.G. and W.D.S. thank D. M. Gill at IBM Research for helpful discussions. W.D.S. and J.K.S.P. are grateful for the financial support of the Natural Sciences and Engineering Research Council of Canada (grant no. STPGP 396995).

#184796 - $15.00 USD Received 5 Feb 2013; revised 5 Apr 2013; accepted 5 Apr 2013; published 12 Apr 2013